

# Thin Animals

*D.A. Johnston*

Dept. of Mathematics  
Heriot-Watt University  
Riccarton  
Edinburgh, EH14 4AS, Scotland

22nd June 1998

## Abstract

Lattice animals provide a discretized model for the  $\theta$  transition displayed by branched polymers in solvent. Exact graph enumeration studies have given some indications that the phase diagram of such lattice animals may contain two collapsed phases as well as an extended phase. This has not been confirmed by studies using other means. We use the exact correspondence between the  $q \rightarrow 1$  limit of an extended Potts model and lattice animals to investigate the phase diagram of lattice animals on  $\phi^3$  random graphs of arbitrary topology (“thin” random graphs). We find that only a two phase structure exists – there is no sign of a second collapsed phase.

The random graph model is solved in the thermodynamic limit by saddle point methods. We observe that the ratio of these saddle point equations give precisely the fixed points of the recursion relations that appear in the solution of the model on the Bethe lattice by Henkel and Seno. This explains the equality of non-universal quantities such as the critical lines for the Bethe lattice and random graph ensembles.

# 1 Introduction

Polymers, whether linear or branched, typically display a two phase structure in solvent with a  $\theta$ -transition [1], whose position depends on temperature and solvent composition, intervening between an extended and a collapsed phase. The case of linear polymers has proved amenable to various analytical treatments such as conformal field theory and Coulomb gas methods [2], but branched polymers have been rather more stubborn.

A discretized model of branched polymers is provided by lattice animals, in essence graphs of connected sites on some lattice. Contact interactions exist between nearest neighbour sites that are not directly linked by a bond of the animal and solvent interactions exist between occupied sites and unoccupied nearest-neighbour sites. All the ingredients of the continuum polymer in solvent problem are thus present. It is known that in  $d$  dimensions the lattice animal exponents are related to those of the Yang-Lee edge singularity in  $d-2$  dimensions which allows the calculation of the bulk entropic exponent for the so-called strongly embedded lattice animal [3]. It is also known that the model corresponds exactly to the  $q \rightarrow 1$  limit of a certain extended  $q$ -state Potts model [4, 5], which has led to the conjecture that a percolation critical point separates two different branches of the  $\theta$  line [6, 7]. More controversially, exact enumeration techniques have suggested that *two* collapsed phases might exist [8] whereas transfer matrix investigations have found no sign of this [7, 9].

This conflict motivated Henkel and Seno [10] to conduct a two-pronged investigation of lattice animals using the extended Potts model formalism. They attacked the infinite dimensional, mean-field problem by solving the model on a Bethe lattice <sup>1</sup> and the low-dimensional problem by using Migdal-Kadanoff [5, 11] recursion relations. In both cases they found only one collapsed phase, and observed that it was unlikely that the topology of the phase diagram would change in intermediate dimensions. In this paper we also use the extended Potts model formalism, this time on  $\phi^3$  random graphs of arbitrary topology, to show that only one collapsed phase exists for these.

A couple of interesting technical points emerge along the way: firstly, ratios of the saddle point equations in the random graph model are isomorphic to the fixed points of the recursion relations that solve the model on the Bethe lattice, so the phase structure on  $\phi^3$  graphs in the large  $n$  limit is identical in all respects to the Bethe lattice; secondly, the symmetry breaking pattern that emerges at the  $\theta$ -transition is not that which one might have naively expected given earlier results for Potts models and percolation on random graphs. The former phenomenon also occurs in other models on random graphs [12, 13, 14] and is heuristically explained by noting that the loops in the random graph model are predominantly large in the thermodynamic limit [15], so the random graphs look locally like the corresponding Bethe lattice and one generically obtains mean field behaviour.

The partition function for lattice animals may be written in several equivalent ways, but we restrict ourselves to that in equ.(1) to facilitate easy comparison with [10]. If an animal contains  $n$  sites,  $b$  bonds and  $k$  contact interactions we can write

$$Z_{animal} = \sum_n x^n Z_n(y, \tau) = \sum_{n,b,k} a_{n,b,k} x^n y^b \tau^k \quad (1)$$

where the site, bond and contact fugacities are given by  $x, y, \tau$  respectively and the  $a$ 's give the number of different animals with the specified numbers of sites, bonds and contacts. There is an exact correspondence between the lattice animal partition function of equ.(1) and the  $q \rightarrow 1$  limit of an extended  $q$  state Potts model [4, 5] with hamiltonian

$$\mathcal{H} = -J \sum_{(i,j)} \delta_{\sigma_i, \sigma_j} - L \sum_{(i,j)} \delta_{\sigma_i, 1} \delta_{\sigma_j, 1} - H \sum_i \delta_{\sigma_i, 1}, \quad (2)$$

where the  $(i, j)$  sums are over nearest neighbour vertices and the spins  $\sigma_i$  take on  $q$  values. The  $\sum_{(i,j)} \delta_{\sigma_i, 1} \delta_{\sigma_j, 1}$  term is non-standard, in its absence we would have the usual Potts hamiltonian (with an external field).

---

<sup>1</sup>Although it might appear at first sight that contact interactions could not be introduced on the loop-less Bethe lattice it should be remembered that the Potts spins encode the animal state, rather than it being related simply to the lattice geometry. If one were really placing an animal on the lattice directly, some sort of cactus lattice would be required to allow such contacts

The Potts model parameters are related to  $x, y$  and  $\tau$  in equ.(1) by

$$x = \exp(-H - \gamma(J + L)), \quad y = (\exp(J) - 1) \exp(J + L), \quad \tau = \exp(J + L) \quad (3)$$

where  $\gamma$  is the coordination number of the lattice or graph on which the animals live, and the partition functions are related by

$$Z_{animal} = \lim_{q \rightarrow 1} \frac{\partial}{\partial q} \ln Z_{Potts} \quad (4)$$

where the Potts partition function is

$$Z_{Potts} = \sum_{\{\sigma\}} \exp(-\mathcal{H}). \quad (5)$$

The idea behind the correspondence is essentially identical to the use of the standard Potts model Hamiltonian in the  $q \rightarrow 1$  limit to describe percolation [16], which is based Fortuin and Kastelyn [17] cluster transcription of Potts and related models.

## 2 Animals on Thin Graphs - Obtaining the Solution

Having discussed the lattice animal model in general we now move on to formulate it on random graphs of arbitrary topology. A particularly economical way of writing down statistical mechanical models on such random graphs was introduced in [18] where it was observed that taking the  $N \rightarrow 1$  limit in the Hermitian matrix models familiar from studies of 2D gravity generated random graphs of arbitrary topology, as opposed to the planar graphs picked out by the  $N \rightarrow \infty$  limit that is used in 2D gravity. The random graphs appear as Feynman diagrams in the perturbative expansion of the partition function. The matrix indices vanish in the  $N \rightarrow 1$  limit, leaving “thin” graphs rather than the fat, or ribbon, graphs of the matrix model proper. We shall denote the non-planar, arbitrary topology random graphs as thin graphs and the animals which live on them as thin animals throughout the rest of the paper for brevity.

In general the partition function of a statistical mechanical model on an ensemble of thin random graphs with  $2m$  vertices is given by

$$Z_m \times N_m = \frac{1}{2\pi i} \oint \frac{d\lambda}{\lambda^{2m+1}} \int \frac{\prod_i d\phi_i}{2\pi \sqrt{\det K}} \exp(-S), \quad (6)$$

where the contour integral over the vertex coupling  $\lambda$  picks out the graphs with  $2m$  vertices,  $S$  is an appropriate action,  $K$  is the inverse of the quadratic form in this action, and the  $\phi_i$  are the various matter variables in the action. As the number of thin random graphs increases factorially with  $m$  the factor  $N_m$  gives the number of undecorated (i.e. without matter) graphs in the class of interest and disentangles this growth from any non-analyticity due to phase transitions. For the  $\phi^3$  (3-regular) random graphs we discuss here

$$N_m = \left(\frac{1}{6}\right)^{2m} \frac{(6m-1)!!}{(2m)!!}. \quad (7)$$

It is perhaps worth emphasising that the  $\phi_i$  appearing in equ.(6) are *scalar* variables, so the evaluation of thin graph partition functions is inherently easier than dealing with the matrix integrals of the planar limit. In the large  $m$ , thermodynamic, limit saddle point methods may be used to evaluate equ.(6). The saddle point equation for  $\lambda$  may be trivialised by scaling it out of the action as an overall factor, leaving any critical behaviour to be revealed by the behaviour of the saddle point equations for the matter fields  $\phi_i$ . Phase transitions are manifested by an exchange of dominant saddle point, either continuously or discontinuously.

We can now write down the action which gives the Boltzmann factors appropriate to the hamiltonian of equ.(2) for a  $q$ -state Potts model on thin  $\phi^3$  random graphs

$$S = \frac{\alpha}{2} \psi^2 + \frac{\beta}{2} \sum_{i=1}^{q-1} \phi_i^2 - \sum_{i=1}^{q-1} \psi \phi_i - \delta \sum_{i>j} \phi_i \phi_j - \frac{\nu}{3} \psi^3 - \sum_{i=1}^{q-1} \frac{1}{3} \phi_i^3 \quad (8)$$

where

$$\begin{aligned}\alpha &= \frac{y}{\tau} + q - 1, \quad \beta = \frac{\tau(y + (\tau - 1)(q - 2))}{y}, \\ \delta &= \frac{\tau(\tau - 1)}{y}, \quad \nu = x^{-1}\tau^{-3},\end{aligned}\tag{9}$$

and we have pre-emptively scaled out the cubic vertex coupling  $\lambda$  as it plays no role in the determination of the phase structure. The inverse of the quadratic form in equ.(8) has the diagonal terms  $(\tau, (y/\tau + 1), (y/\tau + 1), \dots) = (\exp(J + L), \exp(J), \exp(J), \dots)$  with all off-diagonal terms 1, which is precisely what is required. We can also see that when  $L = 0$  we have  $\alpha = \beta = \exp(J) + q - 2$ ,  $\delta = 1$ , and we recover (up to a trivial rescaling) the action for the standard Potts model used in [12].

The saddle point equations for the action in equ.(8) may be solved for increasing  $q$  until patience, or algebraic computing power, run out. “Generic” behaviour sets in at  $q = 4$ , as opposed to  $q = 3$  for the standard action with  $L = 0$ . One finds a disordered phase where  $\psi$  is distinct and the  $q - 1$   $\phi_i$ s are equal to  $\phi$ , which we denote as having  $(1, q - 1)$  symmetry. There are two patterns of symmetry breaking from this phase to ordered states: in the first we have  $\psi$ , one distinct  $\phi_i = \tilde{\phi}$  and the other  $\phi_2 = \phi_3 = \dots = \phi_{q-1}$  equal to  $\phi$ , which we denote as  $(1, 1, q - 2)$ ; in the second we find  $\psi$ ,  $\phi_1 = \phi_2 = \tilde{\phi}$  and  $\phi_3 = \dots = \phi_{q-1} = \phi$  which we denote by  $(1, 2, q - 3)$ . We now follow the path used in the analysis of [12] by writing down effective actions that are sufficient to capture these symmetry breaking patterns. In effect, most of the  $q$  Potts variables are redundant as  $q - 2$  or  $q - 3$  of them are equal in the ordered phases and  $q - 1$  in the disordered phase. Imposing the appropriate symmetries we find the effective actions

$$\begin{aligned}S_{(1,1,q-2)} &= \frac{\alpha}{2}\psi^2 + \frac{\beta}{2}\tilde{\phi}^2 + \frac{(q-2)}{2}\phi^2 \\ &- \psi\tilde{\phi} - (q-2)\psi\phi - \delta \left( \tilde{\phi}\phi(q-2) + \frac{1}{2}(q-2)(q-3)\phi^2 \right) \\ &- \frac{\nu}{3}\psi^3 - \frac{1}{3}\tilde{\phi}^3 - \frac{(q-2)}{3}\phi^3\end{aligned}\tag{10}$$

and

$$\begin{aligned}S_{(1,2,q-3)} &= \frac{\alpha}{2}\psi^2 + \beta\tilde{\phi}^2 + \frac{(q-3)}{2}\phi^2 \\ &- 2\psi\tilde{\phi} - (q-3)\psi\phi - \delta \left( \tilde{\phi}^2 + 2\tilde{\phi}\phi(q-3) + \frac{1}{2}(q-3)(q-4)\phi^2 \right) \\ &- \frac{\nu}{3}\psi^3 - \frac{2}{3}\tilde{\phi}^3 - \frac{(q-3)}{3}\phi^3.\end{aligned}\tag{11}$$

Solving the saddle point equations  $\partial S/\partial\psi = \partial S/\partial\tilde{\phi} = \partial S/\partial\phi = 0$  for either effective action to get  $\psi$ ,  $\tilde{\phi}$ ,  $\phi$  involves only a quadratic equation in the disordered phase, but one is left with a messy quartic to solve in the ordered phase. A direct attack is not very illuminating, but we can use the same legerdemain exercised in [10] for Bethe lattice to simplify the problem greatly. The useful observation made there was that the lattice animal partition function could be written as

$$Z_{\text{animal}} \sim \sum_n (x \exp(F))^n\tag{12}$$

where  $F$  was the canonical ensemble (fixed  $n$ ) free energy. The sum in equ.(12) can be seen to diverge at a critical value of  $x$ , which we denote as  $\tilde{x}$ , which in turn gives the critical canonical ensemble free energy  $F = -\ln \tilde{x}$  of the infinite lattice animal. Therefore, if we can calculate  $\tilde{x}$  as a function of  $y, \tau$  we obtain the canonical free energy

$$F = \lim_{n \rightarrow \infty} n^{-1} \ln Z_n(y, \tau)\tag{13}$$

of the infinite lattice animal as a function of these variables.

To see how this helps, consider the solutions of the saddle point equations obtained from eqs.(10,11) when  $q = 1$ , which are given by

$$\psi = xy\tau^2, \quad \tilde{\Phi}^2 - \tilde{\Phi} + xy = 0, \quad \Phi^2 - \Phi + xy = 0 \quad (14)$$

for both in the disordered phase, with symmetry  $(1, q-1)$ , where  $\tilde{\Phi} = \tilde{\phi}/\tau$ ,  $\Phi = \phi/\tau$  and where we have not solved the quadratics explicitly for reasons that will become apparent below. The ordered phase solutions are obtained from, for equ.(10) with breaking pattern  $(1, 1, q-2)$

$$\begin{aligned} 0 &= \tilde{\Phi}^4 y^2 + 2y[2(1-\tau) - y]\tilde{\Phi}^3 + [4(\tau-1)^2 - 6y(1-\tau) + y^2(1+xy)]\tilde{\Phi}^2 \\ &- [4(1-\tau)^2 + xy^2(2\tau-y) + 2y(\tau-1)]\tilde{\Phi} + [(\tau-1)^2 + \tau xy^2] \end{aligned} \quad (15)$$

$$\Phi = 1 - \tilde{\Phi}$$

$$\psi = -\frac{\tau^2}{y} \left[ y(\tilde{\Phi}^2 - \tilde{\Phi}) - 2(\tau-1)\tilde{\Phi} + (\tau-1) \right]$$

and, for equ.(11) with breaking pattern  $(1, 2, q-3)$

$$\begin{aligned} 0 &= \tilde{\Phi}^4 y^2 + 2y[4(\tau-1) - y]\tilde{\Phi}^3 + [16(\tau-1)^2 + 12y(1-\tau) + y^2(1+xy)]\tilde{\Phi}^2 \\ &- [16(1-\tau)^2 - xy^2(4\tau-y) - 4y(\tau-1)]\tilde{\Phi} + [4(\tau-1)^2 - 2\tau xy^2] \end{aligned} \quad (16)$$

$$\Phi = 1 - \tilde{\Phi}$$

$$\psi = -\frac{\tau^2}{y} \left[ y(\tilde{\Phi}^2 - \tilde{\Phi}) + 4(\tau-1)\tilde{\Phi} - 2(\tau-1) \right].$$

To avoid the onerous task of solving for  $\tilde{\Phi}$  in all of these we now, as advertised, treat equ.(14) and the first of eqs.(15,16) as equations for  $x(y, \tau, \tilde{\Phi})$ , in which variable they are only linear.

### 3 Animals on Thin Graphs - Discussion of the Solution

If we make the substitution  $p = \tilde{\Phi} + 1/2$  to simplify the resulting expressions we find from eqs.(14,15,16)

$$\begin{aligned} x_{1,q-1}(y, p) &= \frac{1 - 4p^2}{4y} \\ x_{1,1,q-2}(y, \tau, p) &= \frac{(1 - 4p^2)^2 y^2 + 16(\tau-1)(1 - 4p^2)py + 64p^2(\tau-1)^2}{4y^2((1 - 4p^2)y + 8p\tau)} \\ x_{1,2,q-3}(y, \tau, p) &= \frac{(1 - 4p^2)^2 y^2 - 32(\tau-1)(1 - 4p^2)py + 256p^2(\tau-1)^2}{4y^2((1 - 4p^2)y - 16p\tau)} \end{aligned} \quad (17)$$

where we have labelled the solutions by their symmetry breaking pattern. We see here the first hint of a close parallel with the Bethe lattice solution of [10] since our two ordered solutions are related by

$$x_{1,2,q-3}(y, \tau, p) = \frac{1}{2} x_{1,1,q-2}\left(\frac{y}{2}, \tau, -p\right), \quad (18)$$

which mirrors a similar symmetry in [10]<sup>2</sup>.

The physical solutions  $\tilde{x}_{1,q-1}(y)$ ,  $\tilde{x}_{1,1,q-2}(y, \tau)$ ,  $\tilde{x}_{1,2,q-3}(y, \tau)$  are obtained by maximising these expressions with respect to  $p$ , which plays the role of an order parameter. The appropriate solution for a given

---

<sup>2</sup>Which does not, however, involve inverting the order parameter.

$(y, \tau)$  is then the largest of these. Bearing in mind that we must have the fugacity  $x$  positive to make sense physically and that the natural ranges of  $y$  and  $\tau$  are  $y \geq 0, \tau \geq 1$ , we see that the physical ranges for  $p$  are  $0 \leq p \leq 1/2$  for  $x_{1,1,q-1}$ ,  $-1/2 \leq p \leq 0$  for  $x_{1,2,q-3}$  and  $-1/2 \leq p \leq 1/2$  for  $x_{1,q-1}$ .

At this point it might appear that we have succeeded in showing precisely the reverse of what was announced in the introduction in that we have found *two* candidate ordered phases, which might be identified with the two contentious collapsed polymer phases. However, an extensive numerical investigation throughout the  $(y, \tau)$  range reveals that the one of the solutions,  $\tilde{x}_{1,2,q-3}(y, \tau)$ , is always larger than the other,  $\tilde{x}_{1,1,q-2}(y, \tau)$ , for a given  $(y, \tau)$  so it is the former which is always dominant.

For the disordered solution we clearly have a maximum at  $p = 0$

$$\tilde{x}_{1,q-1}(y) = \frac{1}{4y}, \quad (19)$$

so the free energy is  $F = \ln(4y)$  and we also find

$$x_{1,1,q-2}(y, \tau, 0) = x_{1,2,q-3}(y, \tau, 0) = \frac{1}{4y}. \quad (20)$$

We are now in a position to map out the phase structure of thin animals. We have found two phases, whose free energies are given by  $F = -\ln \tilde{x}_{1,q-1}(y)$  which we can identify with the extended phase and  $F = -\ln \tilde{x}_{1,2,q-3}(y, \tau)$  which we identify with the (single) collapsed phase.

The transition line between these two phases may be pinned down by noting that

$$\frac{\partial x_{1,2,q-3}(y, \tau, p)}{\partial p} = 0 \quad (21)$$

iff  $\tau = 2$ . We then observe that

$$\frac{\partial^2 x_{1,2,q-3}(y, 2, 0)}{\partial p^2} = 2 \frac{64 - y^2}{y^3} \quad (22)$$

so  $\tilde{x}_{1,2,q-3}(y, 2, p)$  has a maximum at  $p = 0$  if  $y > 8$ , a minimum if  $y < 8$  and a turning point if  $y = 8$ . A glance at Figs.1,2 where we plot  $x_{1,q-1}(y, p)$  and  $x_{1,2,q-3}(y, 2, p)$  for  $y = 10$  and  $y = 4$  respectively clarifies what is going on. In Fig.1 we see that  $x_{1,q-1}(y, p)$  and  $x_{1,2,q-3}(y, 2, p)$  share a common maximum at  $p = 0$  when  $y = 10$  (which is the case for all  $y \geq 8$ ), whereas for  $y = 4$  the maximum of  $x_{1,2,q-3}(y, 2, p)$  lies at some  $p < 0$ . This means that we see a continuous transition as  $\tau$  is varied across  $\tau = 2$  when  $y > 8$  between extended animals at small  $\tau$  and collapsed animals at large  $\tau$ . For  $y < 8$  the position of the critical line in the  $(y, \tau)$  plane must be determined numerically and the transition is first order. The physical solution jumps discontinuously from the maximum of  $x_{1,q-1}$  at  $p = 0$  to the maximum of  $x_{1,2,q-3}$  at  $p < 0$ . The appropriate equations for pinpointing the first order line are thus

$$\begin{aligned} x_{1,2,q-3}(y, \tau, p) = x_{1,q-1}(y, 0) &= \frac{1}{4y} \\ \frac{\partial x_{1,2,q-3}(y, \tau, p)}{\partial p} &= 0 \\ \frac{\partial^2 x_{1,2,q-3}(y, \tau, p)}{\partial p^2} &\leq 0 \end{aligned} \quad (23)$$

which give the conditions for the maximum in  $x_{1,2,q-3}(y, \tau, p)$  at  $p < 0$  to be equal to the maximum in  $x_{1,q-1}(y, p)$  at  $p = 0$ .

A triple point at  $y = 8, \tau = 2$  separates the first and second order transition lines. All of these features are indicated in the schematic phase diagram of Fig.3. The presence of a jump across the first order line is confirmed explicitly by the sample values in Figs.4,5 where we see that as we cross the line by varying  $\tau$  at fixed  $y = 4$  we move from  $x_{1,q-1}$  dominant in Fig.4 to the situation in Fig.5 where  $x_{1,2,q-3}$  is just equal to the maximum of  $x_{1,q-1}$  ( $1/4y$  at the origin) for a *non-zero*  $p$  value ( $\simeq -0.1634\dots$ ) at  $\tau \simeq 1.8528\dots$ . At this point  $p$  jumps discontinuously and we move into the collapsed phase as  $\tau$  increases.

When moving across the second order portion of the line however, the maximum of  $x_{1,2,q-3}$  is at the origin and we see no jump in  $p$ , giving a second order transition. This can be seen by referring back to

Fig.1 and comparing it with Fig.6. In Fig.6 we are *below* the second order line at  $y = 10, \tau = 1$  and the two curves look much like Fig.4. As we move up to the line at  $y = 10, \tau = 2$  in Fig.1 we can see that the maximum of  $x_{1,2,q-3}$  now lies at the origin and increasing  $\tau$  further takes us into the collapsed phase via a second order transition.

In closing this section it should be remarked that although the broad features of the random graph phase diagram appear to be in accordance with two-dimensional models, there is one notable difference. The triple point separating the first and second order portions of the  $\theta$  line is the percolation point in  $2D$ . That is *not* the case here – the percolation point in the random graph model is at  $L = H = 0$  and  $\tau = 2$ , which in turn implies  $y = \tau(\tau - 1) = 2^3$ . This presumably can be ascribed to the mean-field nature of the model, a comment which also applies to the Bethe lattice results of [10], whose similarities with the work here we now move on to discuss.

## 4 Comparison with Bethe Lattice results

Anyone familiar with the results of [10] for Bethe lattice animals may at this point be experiencing a strong sense of déjà vu. The thin animal phase diagram has proved to be identical to that on the Bethe lattice, down to non-universal quantities such as the position of the  $\theta$  line and triple point. As we have already noted, even before extracting the physical solutions  $\tilde{x}$  parallels are apparent since the two ordered solutions on both random graphs and the Bethe lattice possess a particular  $y \rightarrow y/2$  symmetry. Our criteria for extracting the  $\theta$  line are also identical to those used on the Bethe lattice, although the equations for  $x$  on the Bethe lattice are quadratic rather than linear, as above. All this clearly begs an explanation.

Our saddle point equations for  $x_{1,2,q-3}$  at  $q = 1$ , which we have so far not written explicitly, are given by

$$\begin{aligned}\psi^2 &= xy\tau^2\psi - 2x\tau^3\tilde{\phi} + 2x\tau^3\phi \\ \tilde{\phi}^2 &= -\psi - \frac{2\tau(\tau-1) - \tau y}{y}\tilde{\phi} + \frac{2\tau(\tau-1)}{y}\phi \\ \phi^2 &= -\psi - \frac{2\tau(\tau-1)}{y}\tilde{\phi} + \frac{2\tau(\tau-1) + \tau y}{y}\phi.\end{aligned}\tag{24}$$

At first sight these bear little relation to the fixed points of the recursion relations used in [10] to obtain the dominant solution to the model on the Bethe lattice.

The method of derivation is certainly completely different. On the Bethe lattice one considers the behaviour of the central spin  $\sigma_0$  [10], writing

$$Z_{Potts} = \sum_{\sigma_0} \exp(H\delta_{\sigma_0,1}) \sum_{\{s\}} \prod_{j=1}^3 Q_n(\sigma_0|s^{(j)})\tag{25}$$

where  $s^{(j)}$  is the spin on the  $j$ th sub-branch and

$$Q_n(\sigma_0|s^{(j)}) = \exp(J\delta_{\sigma_0,s_1} + L\delta_{\sigma_0,1}\delta_{s_1,1} + H\delta_{\sigma_0,1}) \exp\left(J\sum'_{(i,j)}\delta_{s_i,s_j} + L\sum'_{(i,j)}\delta_{s_i,1}\delta_{s_j,1} + H\sum'_i\delta_{s_i,1}\right)\tag{26}$$

and the primed sums are over the sub-branch with first spin  $s_1$ . The solution then follows by defining

$$g_n(\sigma_0) = \sum'_{\{s\}} Q_n(\sigma_0|s),\tag{27}$$

where  $n$  labels the “shell” of the Bethe lattice, and noting that it satisfies the recursion relation

$$g_n(\sigma_0) = \sum_{s_1=1}^q \exp(J\delta_{\sigma_0,s_1} + L\delta_{\sigma_0,1}\delta_{s_1,1} + H\delta_{s_1,1}) (g_{n-1}(s_1))^2.\tag{28}$$

---

<sup>3</sup>Remarkably, the same numerical values as the  $2D$  model.

Defining

$$\Theta_n = \frac{g_n(\sigma_0 \neq 1, 2)}{g_n(1)}, \quad Z_n = \frac{g_n(2)}{g_n(1)} \quad (29)$$

and taking the limit  $n \rightarrow \infty$  allows one to write the fixed point of the recursion relations in equ.(28) as

$$\begin{aligned} \Theta &= \frac{x^{-1}\tau^{-3} + 2Z^2 + (\frac{y}{\tau} - 2)\Theta^2}{x^{-1}\tau^{-2} + 2Z^2 - 2\Theta^2} \\ Z &= \frac{x^{-1}\tau^{-3} + (\frac{y}{\tau} + 2)Z^2 - 2\Theta^2}{x^{-1}\tau^{-2} + 2Z^2 - 2\Theta^2} \end{aligned} \quad (30)$$

where  $\Theta = \lim_{n \rightarrow \infty} \Theta_n$ ,  $Z = \lim_{n \rightarrow \infty} Z_n$ .

Given the identical phase diagram we have found on random graphs to the Bethe lattice results of [10] it is clear that the two sets of equations, eqs.(24, 30), must somehow be equivalent. This can be made explicit by a simple transformation. Eqs.(24) may be symbolically written as  $\vec{\phi}^2 = A\vec{\phi}$ , where  $\vec{\phi}$  is the column vector  $(\psi, \tilde{\phi}, \phi)$  and  $\vec{\phi}^2$  is  $(\psi^2, \tilde{\phi}^2, \phi^2)$ . We are at liberty to rewrite these as  $\vec{\phi} = A^{-1}\vec{\phi}^2$  as  $A$  is invertible in general

$$\begin{aligned} \psi &= \frac{1}{\tau^2 xy} \psi^2 + \frac{2}{y} \tilde{\phi}^2 - \frac{2}{y} \phi^2 & (a) \\ \tilde{\phi} &= \frac{1}{\tau^3 xy} \psi^2 + \frac{y + 2\tau}{\tau y} \tilde{\phi}^2 - \frac{2}{y} \phi^2 & (b) \\ \phi &= \frac{1}{\tau^3 xy} \psi^2 + \frac{2}{y} \tilde{\phi}^2 + \frac{y - 2\tau}{\tau y} \phi^2 & (c). \end{aligned} \quad (31)$$

If we now divide (c)/(a) and (b)/(a)

$$\begin{aligned} \frac{\phi}{\psi} &= \frac{x^{-1}\tau^{-3}\psi^2 + 2\tilde{\phi}^2 + (\frac{y}{\tau} - 2)\phi^2}{x^{-1}\tau^{-2}\psi^2 + 2\tilde{\phi}^2 - 2\phi^2} \\ \frac{\tilde{\phi}}{\psi} &= \frac{x^{-1}\tau^{-3}\psi^2 + (\frac{y}{\tau} + 2)\tilde{\phi}^2 - 2\phi^2}{x^{-1}\tau^{-2}\psi^2 + 2\tilde{\phi}^2 - 2\phi^2} \end{aligned} \quad (32)$$

and make the identifications

$$\Theta = \frac{\phi}{\psi}, \quad Z = \frac{\tilde{\phi}}{\psi} \quad (33)$$

we obtain exactly the two recursion equation fixed points of equ.(30).

Although we have two distinct physical systems, closed random graphs of arbitrary topology which *do* contain loops, and the loop-less Bethe lattice the preceding calculation shows that the thermodynamic behaviour of lattice animals on both is identical. In a precise sense the loops do not matter, as the saddle point equations that govern the random graph thermodynamic limit are isomorphic to the recursion relations that arise in solving the loop-less Bethe lattice. The identity between the Bethe lattice recursion relations and ratios of the random graph saddle point equations also occurs for other systems (standard Ising, Potts spins etc.) [14], where the consequences are the same, namely the random graph solutions are identical to those on the Bethe lattice.

## 5 Discussion

The astute reader might remark that the solution of the lattice animal problem on random graphs presented in this paper does not really provide any further evidence against the existence of a second collapsed phase, as we have also shown that the solutions to the model have the same content as the Bethe lattice solution in [10], though this is an interesting result in itself. One could counter the objection by stating that we have found a different physical system, and solved it by very different means, in order to arrive at these conclusions.



The thin graph solution also clarifies one lacuna in the Bethe lattice approach. As we have noted, solving the full set of saddle point equations  $\partial S/\partial\psi = \partial S/\partial\phi_i = 0$  (i.e. *before* going to the effective actions) shows that only one disordered and two ordered phases<sup>4</sup> are present for arbitrary  $q$ . On the Bethe lattice enough order parameters are introduced by hand to distinguish the two putative ordered phases, which is then shown to be self-consistent. The possibility of a more exotic phase diagram is not, however, explicitly excluded. The random graph saddle point equations show that this really is enough, as no other patterns of symmetry breaking are observed for any  $q$ .

The observed symmetry breaking pattern itself on random graphs is unexpected, namely  $(1, q-1) \rightarrow (1, 2, q-3)$ . For the standard  $q$ -state Potts model one has  $(q) \rightarrow (1, q-1)$ , so the pattern observed for the sub-dominant solution  $(1, q-1) \rightarrow (1, 1, q-2)$  might have been a more obvious first guess. We have also remarked that the critical percolation point,  $y = \tau = 2$  on thin graphs, is not equal to the tricritical point  $y = 8, \tau = 2$  that separates the two portions of  $\theta$  line, in contrast to the  $2D$  model, although the general topology of the phase diagram is similar.

Although the work presented in this paper is fairly self-contained one obvious generalisation suggests itself. The action of equ.(8) will also serve to represent lattice animals on *planar* random graphs if one takes the  $\psi, \phi_i$  to be  $N \times N$  Hermitian matrices and performs the limit  $N \rightarrow \infty$ . The  $L = H = 0$  case (percolation) has already been solved by Kazakov [19], which suggest that the animal problem might also be tractable. The interest in doing this is that it could shed light on a another vexed question for animals – the (lack of) conformal invariance in the  $2D$  model.

As a technical point, sidestepping the solution of difficult saddle point equations by considering the canonical free energy and solving for the fugacity associated with the external field is an idea which might also be fruitfully applied to the solution of the standard Potts (or even Ising) models in an external field on random graphs, where similarly complicated equations arise.

I would like to thank Malte Henkel for helpful discussions, both in person and electronically.

---

<sup>4</sup>One of which is always dominant.

## References

- [1] P.G. de Gennes, *Scaling Concepts in Polymer Physics*, Cornell University Press (1979)
- [2] J.L. Cardy, “Conformal Invariance and Statistical Mechanics” in *Fields, Strings and Critical Phenomena*, Les Houches XLIX, E. Brézin and J. Zinn-Justin Eds, North Holland Amsterdam (1990);  
P. Christe and M. Henkel, *Introduction to Conformal Invariance and its Applications to Critical Phenomena*, Springer Verlag Heidelberg (1993);  
B. Nienhuis, “Coulomb gas formulation of two dimensional phase transitions” in *Phase transitions and Critical Phenomena* vol 11, C. Domb and J.L. Lebowitz Eds, Academic Press (1987);  
B. Duplantier and H. Saleur, Phys. Rev. Lett. **59**, 539 (1987);  
C. Vanderzande, A.L. Stella and F. Seno, Phys. Rev. Lett. **67**, 2757 (1991)
- [3] G. Parisi and N. Sourlas, Phys. Rev. Lett. **46**, 871 (1981)
- [4] M. Giri, M.J. Stephen and G.S. Grest, Phys. Rev. B16, 4971 (1977);  
F.Y. Wu, J. Stat. Phys. **18**, 115 (1978); Rev. Mod. Phys. **54**, 235 (1982);
- [5] A. Coniglio, J. Phys. **A16**, L187 (1983)
- [6] S. Flesia, D.S. Gaunt, C.E. Soteris and S.G. Whittington, J. Phys. **A25**, L1169 (1992);  
C. Vanderzande, Phys. Rev. Lett. **70**, 3595 (1993)
- [7] F. Seno and C. Vanderzande, J. Phys. **A27**, 5813 (1994); Corr. **A27**, 7937 (1994)
- [8] N. Madras, C.E. Soteris, S.G. Whittington, J.L. Martin, M.F. Sykes, S. Flesia and D.S. Gaunt, J. Phys. **A23**, 5327 (1990);  
I.S. Chang and Y. Shapir, Phys. Rev. **B38**, 6736 (1988)
- [9] B. Derrida and H.J. Herrmann, J. Physique **44**, 1365 (1983);  
B. Derrida and L. De Seze, J. Physique **43**, 475 (1982)
- [10] M. Henkel and F. Seno, Phys. Rev. **E53**, 3662 (1996)
- [11] T.W. Burkhardt and J.M.J. van Leeuwen, “Progress and Problems in Real-Space Renormalization” in *Real Space Renormalization*, T.W. Burkhardt and J.M.J. van Leeuwen Editors, Springer-Verlag (1982), p. 1;  
T.W. Burkhardt, “Bond-Moving and Variational Methods in Real-Space Renormalization”, *ibid.*, p. 33
- [12] D. Johnston and P. Plecháč, J. Phys. **A30** (1997) 7349.
- [13] C. Baillie, D. Johnston and J-P. Kownacki, Nucl. Phys. **B432** (1994) 551;  
C. Baillie, W. Janke, D. Johnston and P. Plecháč, Nucl. Phys. **B450** (1995) 730;  
C. Baillie and D. Johnston, Nucl. Phys. **B47** (Proc. Suppl.) (1996) 649;  
C. Baillie, N. Dorey, W. Janke and D. Johnston, Phys. Lett **B369** (1996) 123.
- [14] D. Johnston and P. Plecháč, J. Phys. **A31** (1998) 475.
- [15] B. Bollobás, “Random Graphs”, Academic Press, 1985.
- [16] F. Peruggi, J. Phys. **A16** (1983) L713.  
F. Peruggi, F. di Liberto and G. Monroy, J. Phys. **A16** (1983) 811;  
F. Peruggi, Physica **141A** (1987) 140;  
F. Peruggi, F. di Liberto and G. Monroy, Physica **141A** (1987) 151;  
J. Essam, J-C Lin and P. Taylor, Phys. Rev. **E52** (1995) 44;  
F. Peruggi, F. di Liberto and G. Monroy, Z. Phys. **B66**, (1987) 379.

- [17] C. Fortuin and P. Kasteleyn, *Physica* **57** (1972) 536;  
P. Kasteleyn and C. Fortuin, *J. Phys. Soc. Jpn (Suppl.)* **26** (1969) 11.
- [18] C. Bachas, C. de Calan and P. Petropoulos, *J. Phys.* **A27** (1994) 6121.
- [19] V. Kazakov, *Mod. Phys. lett.* **A4** (1989) 1691.

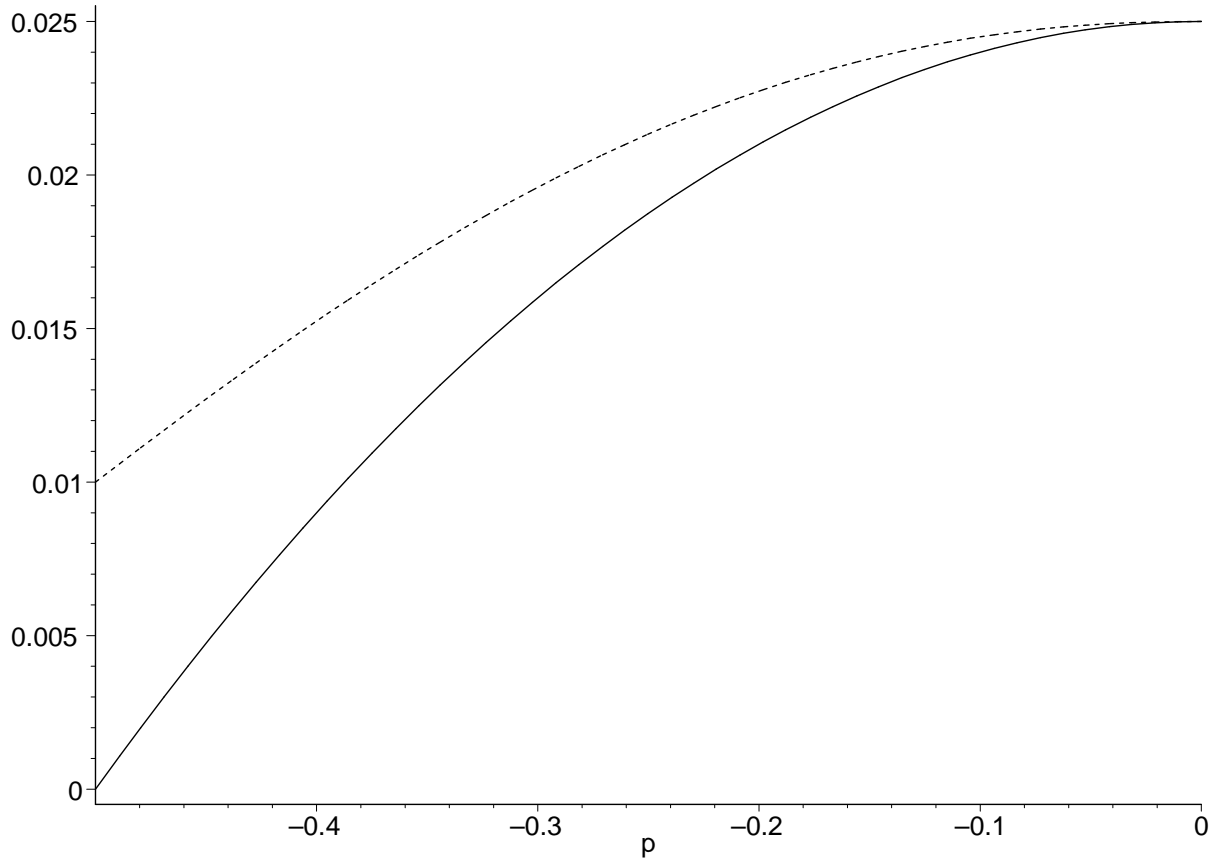


Figure 1: The two solutions vs  $p$  when  $\tau = 2, y = 10$ . The upper dotted curve is  $x_{1,2,q-3}$  and the lower bold curve is  $x_{1,q-1}$ . The maximum of both curves lies at  $p = 0$ .

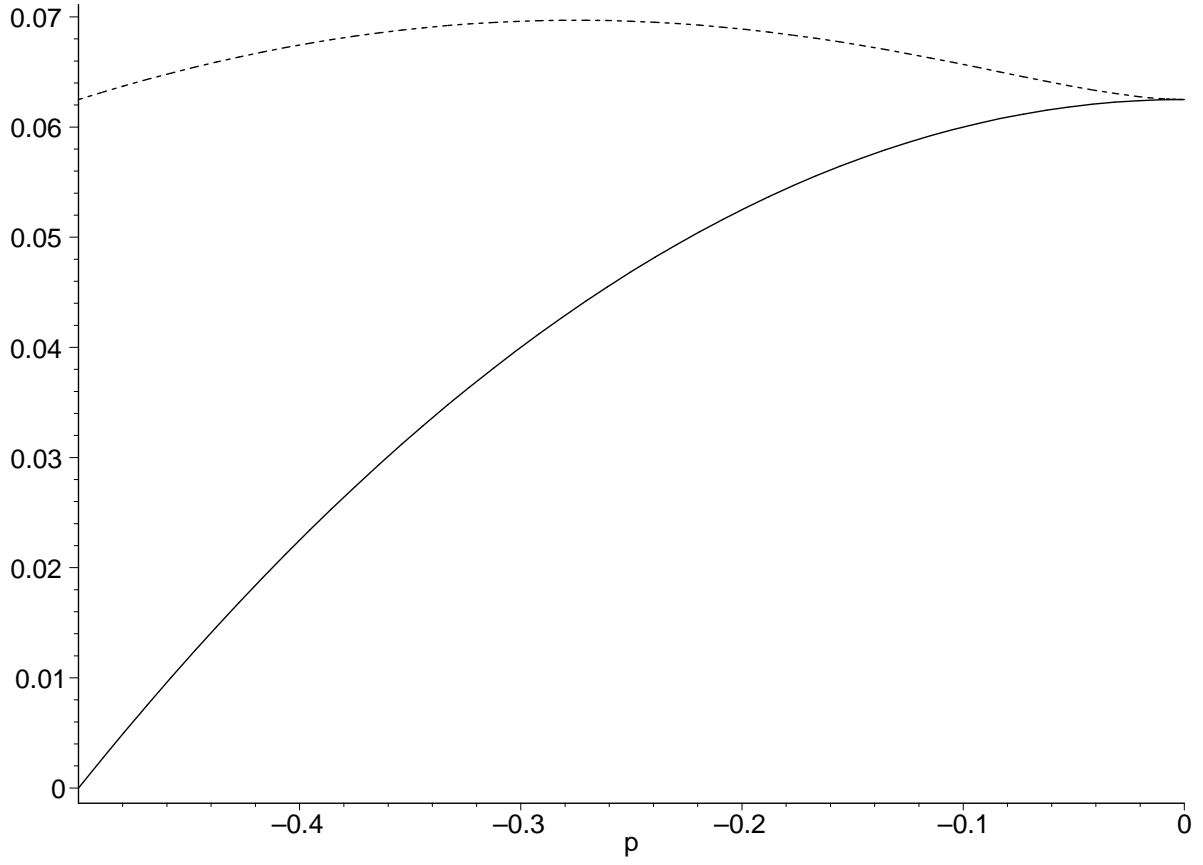


Figure 2: The two solutions vs  $p$  when  $\tau = 2, y = 4$ . Again, the upper dotted curve is  $x_{1,2,q-3}$  and the lower bold curve  $x_{1,q-1}$ . The maximum of  $x_{1,2,q-3}$  now lies away from  $p = 0$ , signalling a first order transition.

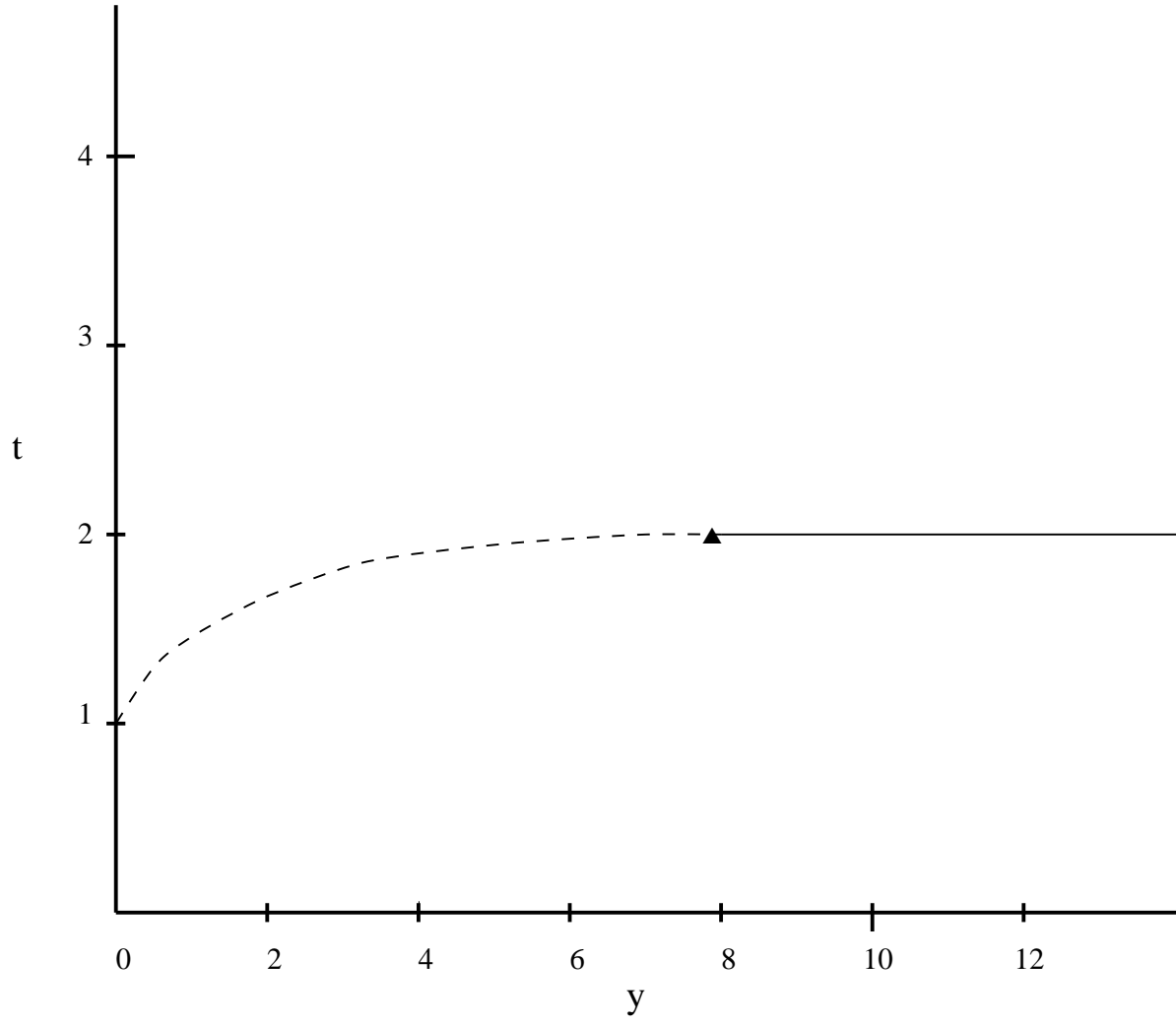


Figure 3: The (schematic) phase diagram for thin animals. The solid line  $\tau = 2, y > 8$  is a line of second order transitions, whereas the dashed line is first order. The triple point is shown at  $y = 8, \tau = 2$  at the meeting point of the two.

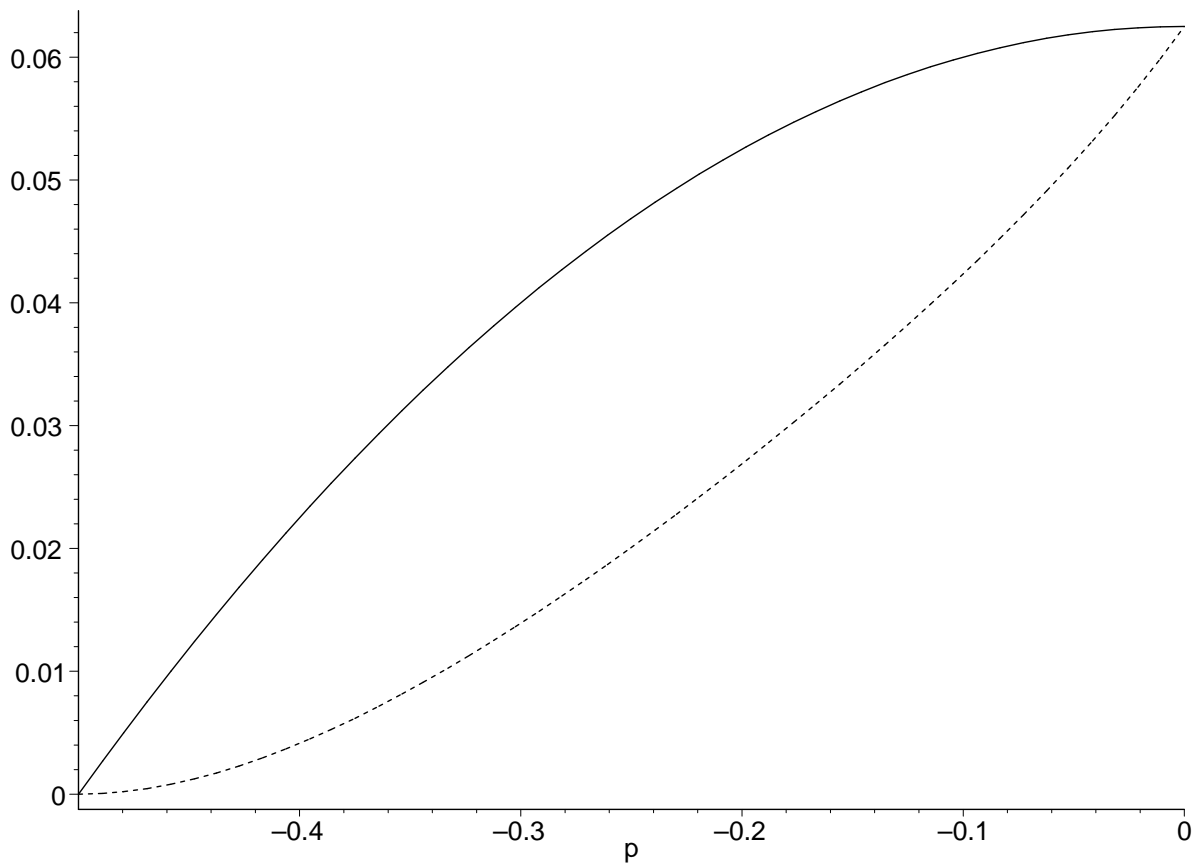


Figure 4: The two solutions *below* the first order portion of the critical line at  $y = 4, \tau = 1$ .  $x_{1,q-1}$  is shown in bold,  $x_{1,2,q-3}$  dotted.

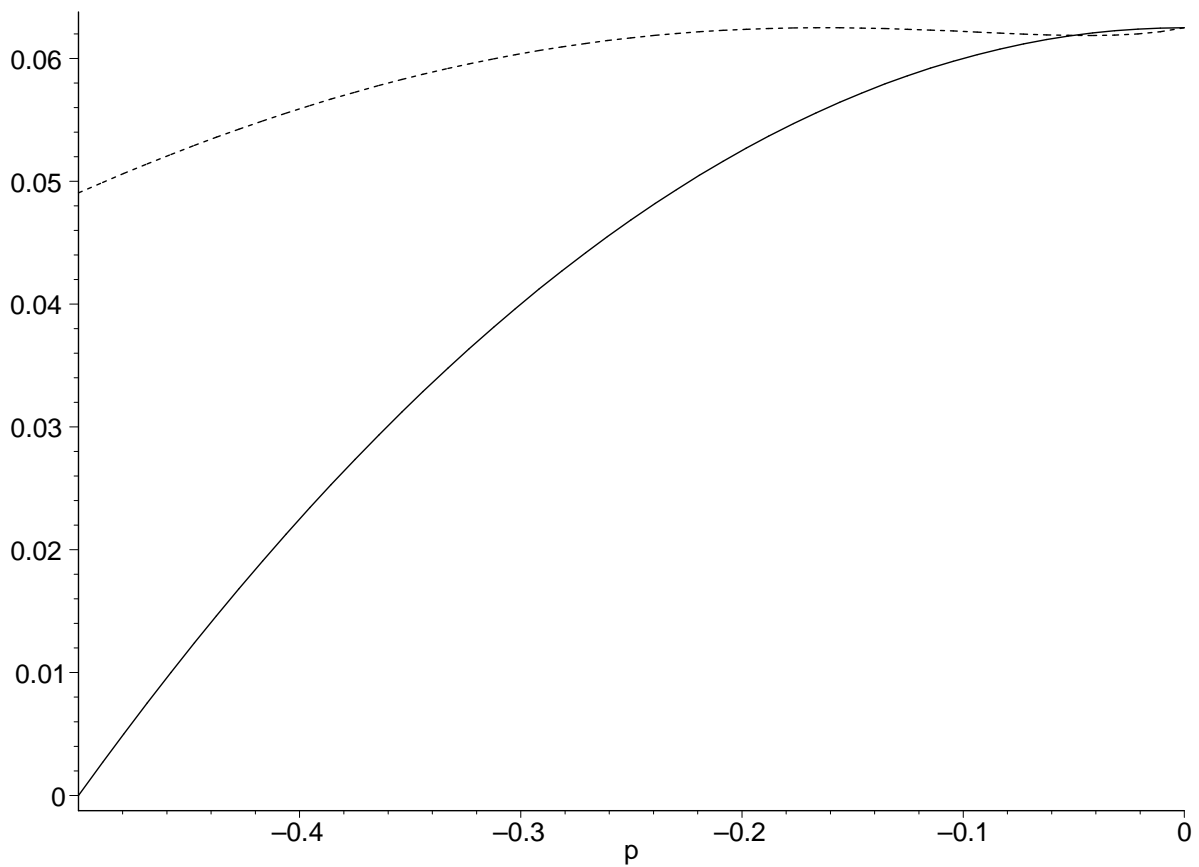


Figure 5: The solutions on the first order portion of the critical line at  $y = 4, \tau \simeq 1.8528 \dots$   $x_{1,2,q-3}$  is shown dotted and its maximum at  $p \simeq -0.1634 \dots$  has just reached  $1/4y$ .  $x_{1,q-1}$ , shown in bold, has the same maximum at  $p = 0$ .



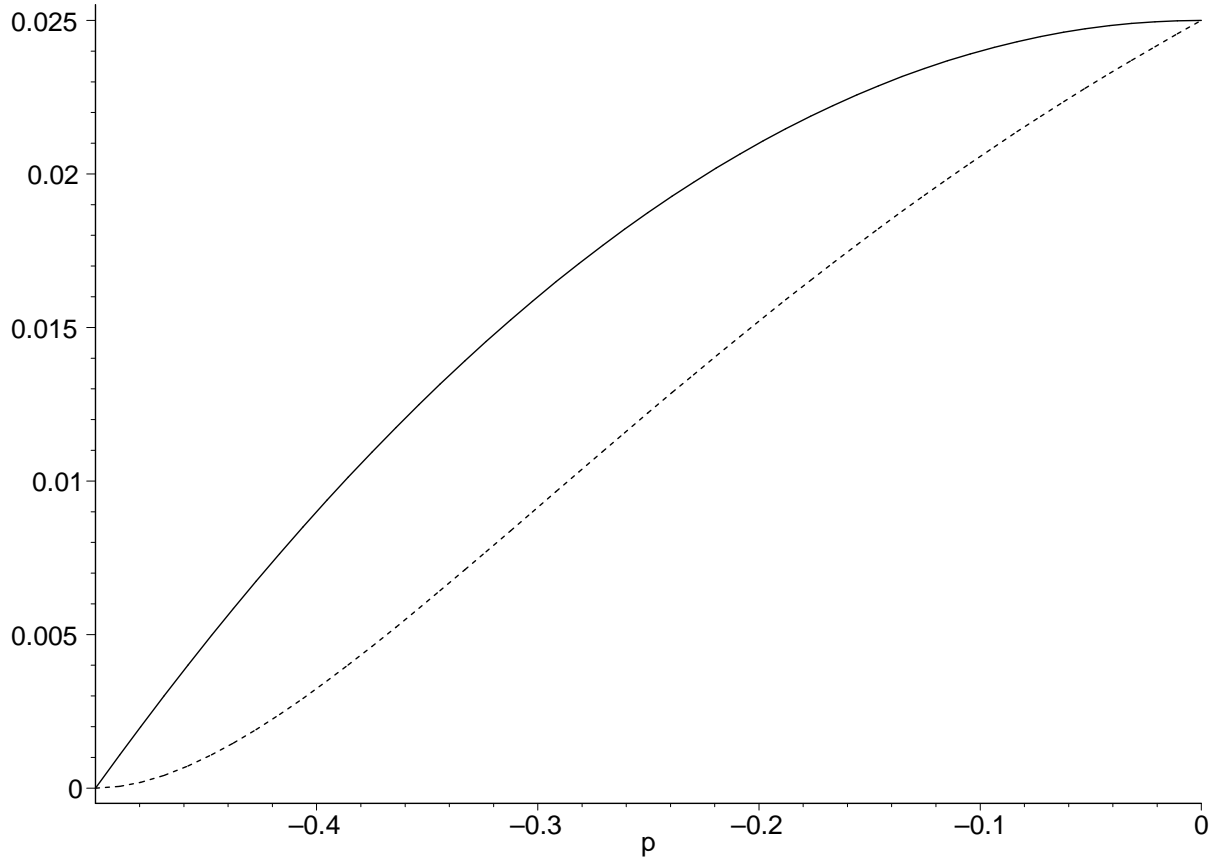


Figure 6: The two solutions *below* the second order portion of the critical line at  $y = 10, \tau = 1$ .  $x_{1,q-1}$ , again denoted by a solid line, is dominant.